

Closing the Loop: Joint Rain Generation and Removal via Disentangled Image Translation *Supplementary Material*

Yuntong Ye^{1,2}, Yi Chang^{2,*}, Hanyu Zhou¹, Luxin Yan¹

¹National Key Laboratory of Science and Technology on Multispectral Information Processing,
School of Artificial Intelligence and Automation, Huazhong University of Science and Technology, China

²AI Center, Peng Cheng Laboratory, Shenzhen, China

{yuntongye, yichang, hyzhou, yanluxin}@hust.edu.cn

In this supplementary, we first provide visualize our generated real rainy images in Section 1, which demonstrate the effectiveness of the generation sub-network in JRGR. We then show more qualitative comparisons in Section 2. In Section 3, we visualize the results in ablation study to further illustrate the effectiveness of losses.

1. Rain Generation

We show the visualization results of the generated real rainy images in Fig. 1 to show the effectiveness of the real rain generation sub-network. Taking the advantage of disentangled translation, the real rain generator in JRGR can focus on the real rain layers to learn more factors in real-world scene such as rain accumulation and blurring, which are difficult to precisely describe in a hand-crafted model. Thus, as a byproduct of JRGR, we generate more realistic rainy images, which further benefits the real rain removal.

2. Qualitative Comparisons

We provide more qualitative comparisons on RainRendering [2] [Fig. 3 - 7], RainHQ [5] [Fig. 9 - 13] and our collected RealRain [Fig. 15 - 19] with (1) supervised methods: DDN [1], JORDER-E [7], RESCAN [4], (2) semi-supervised methods: SSIR [6], Syn2Real [8] and (3) unsupervised method Cycle GAN [9]. Fig. 2, 8, 14 illustrate the experiment settings.

On the synthetic datasets, the disentanglement of background in JRGR is very effective because of the background similarity of paired data and unpaired data, which leads to the best performance in comparisons. On the real rain dataset RainHQ and RealRain, the rain streaks are more complex. Cycle GAN dose not focus on the rain in image translation, thus generates unnatural deraining results.

SSIR and Syn2Real obtain comparable results in some testing examples by their ability of transfer learning. JRGR removes most of the rain by learning the real rain streaks in both removal and generation procedures, while preserve the backgrounds via disentanglement.

3. Ablation Study

To illustrate the effectiveness of different losses, we show the visualization results in the ablation study in Fig. 20, 21, 22. The adversarial losses aim to guarantee the domain of outputs. Without the adversarial losses, the rain removal sub-network does not necessarily decompose the rainy images into the domain of clean backgrounds, thus leaving the rain streaks and generating artifacts [Fig. 20, 21, 22 (a)]. Without the cycle-consistency losses, the content information of rainy images is destroyed in the network due to the lack of supervision [Fig. 20, 21, 22 (b)]. The MSE losses have relatively less influence to the real rain removal results [Fig. 20, 21, 22 (c)], which are mainly imposed for the synthetic rain removal sub-network.

References

- [1] X. Fu, J. Huang, D. Zeng, Y. Huang, X. Ding, and J. Paisley. Removing rain from single images via a deep detail network. In *IEEE Conf. Comput. Vis. Pattern Recog.*, pages 3855–3863, 2017. 1
- [2] S. Halder, J. Lalonde, and R. Charette. Physics-based rendering for improving robustness to rain. In *Int. Conf. Comput. Vis.*, pages 10203–10212, 2019. 1, 4
- [3] X. Hu, C. Fu, L. Zhu, and P. Heng. Depth-attentional features for single-image rain removal. In *IEEE Conf. Comput. Vis. Pattern Recog.*, pages 8022–8031, 2019. 4
- [4] X. Li, J. Wu, Z. Lin, H. Liu, and H. Zha. Recurrent squeeze-and-excitation context aggregation net for single image deraining. In *Eur. Conf. Comput. Vis.*, pages 254–269, 2018. 1

*Corresponding Author

- [5] T. Wang, X. Yang, K. Xu, S. Chen, Q. Zhang, and R. Lau. Spatial attentive single-image deraining with a high quality real rain dataset. In *IEEE Conf. Comput. Vis. Pattern Recog.*, pages 12270–12279, 2019. [1](#), [7](#)
- [6] W. Wei, D. Meng, Q. Zhao, Z. Xu, and Y. Wu. Semi-supervised transfer learning for image rain removal. In *IEEE Conf. Comput. Vis. Pattern Recog.*, pages 3877–3886, 2019. [1](#)
- [7] W. Yang, R. Tan, J. Feng, Z. Guo, S. Yan, and J. Liu. Joint rain detection and removal from a single image with contextualized deep networks. *IEEE Trans. Pattern Anal. Mach. Intell.*, 42(6):1377–1393, 2019. [1](#)
- [8] R. Yasarla, V. Sindagi, and V. Patel. Syn2real transfer learning for image deraining using gaussian processes. In *IEEE Conf. Comput. Vis. Pattern Recog.*, pages 2726–2736, 2020. [1](#)
- [9] J. Zhu, T. Park, P. Isola, and A. Efros. Unpaired image-to-image translation using cycle-consistent adversarial networks. In *Int. Conf. Comput. Vis.*, pages 2223–2232, 2017. [1](#)

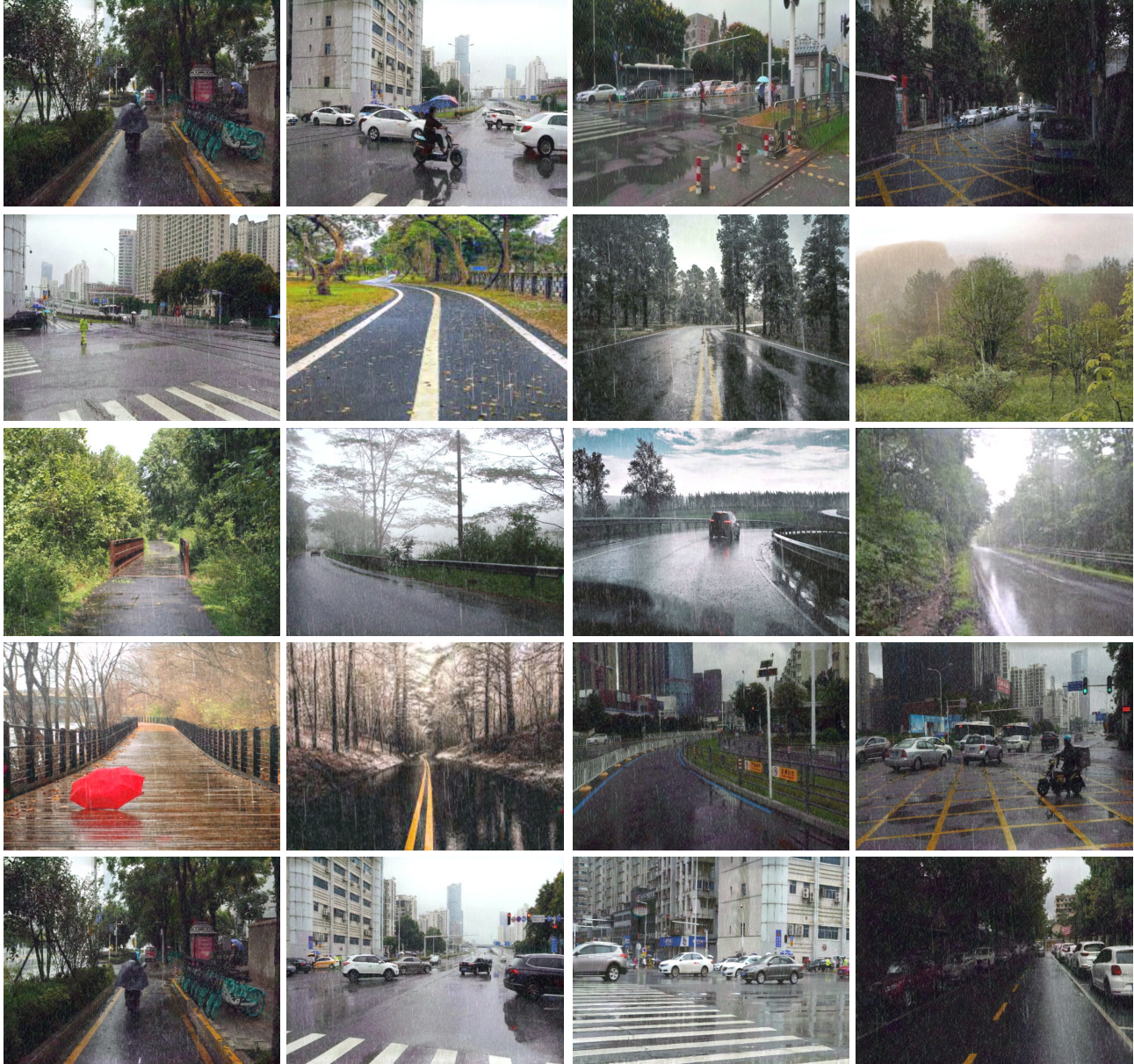


Figure 1. Visualization results of generated rainy images in JRGR which show the effectiveness of the real rain generation sub-network. The rain generator in JRGR learns more factors in real-world scene such as rain accumulation and blurring which are difficult to precisely describe in a hand-crafted model, thus generating more realistic rainy images.



Figure 2. Illustration of our training data. For supervised methods, we utilize (a) paired data on RainCityscape [3] to train the models and test them in (b) unpaired data on Rendering [2]. For semi-supervised methods, we train the models with (a) and (b), and test them in (b). For unsupervised methods, we train the models with (b) and the clean images in (a), and test them in (b).

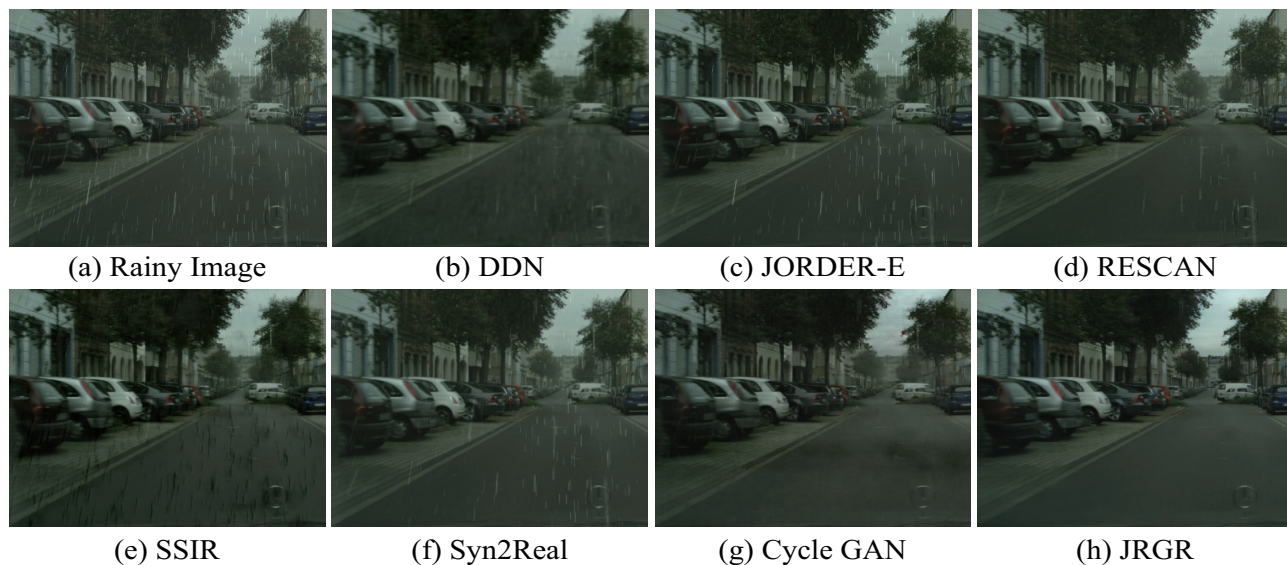


Figure 3. Visualization of deraining results on Rendering dataset.

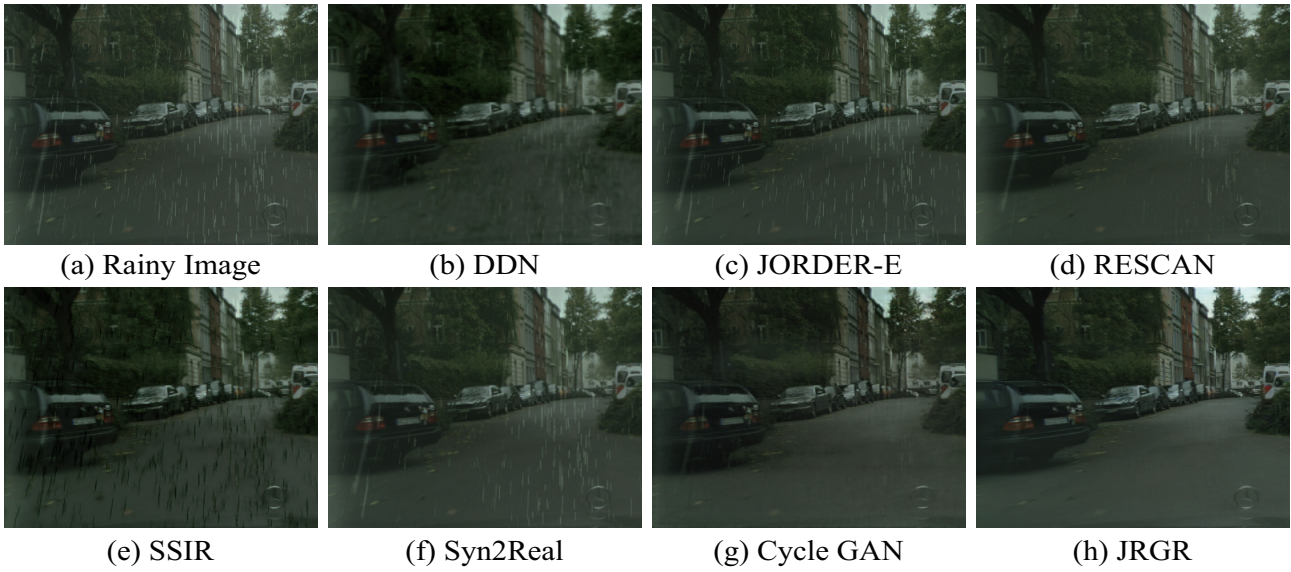


Figure 4. Visualization of deraining results on Rendering dataset.

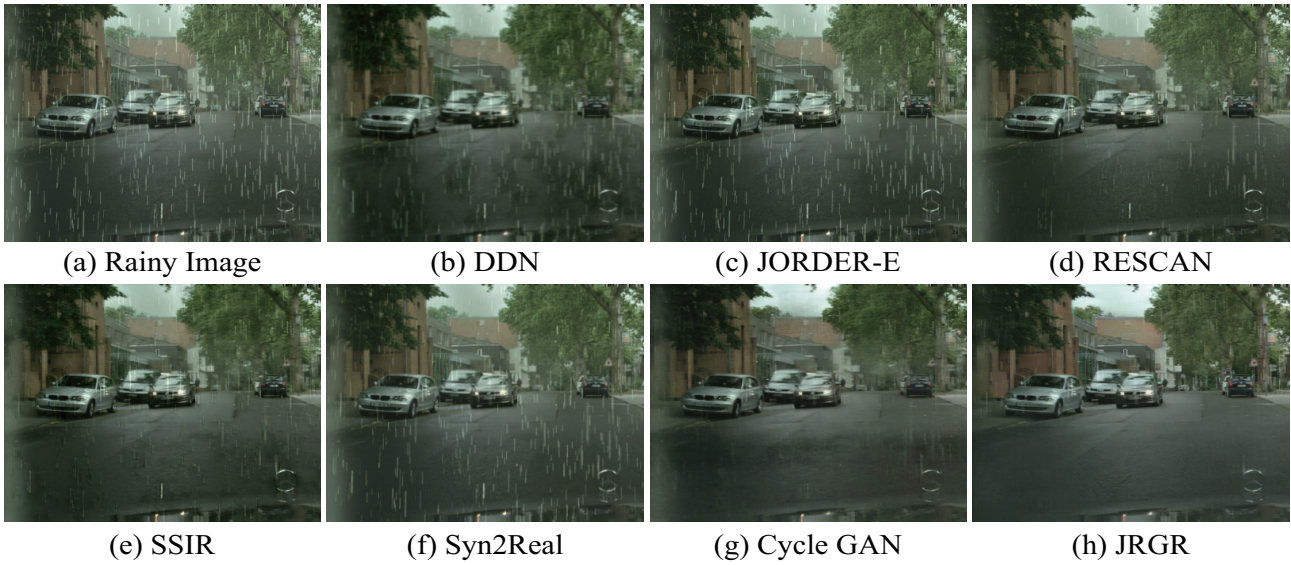


Figure 5. Visualization of deraining results on Rendering dataset.

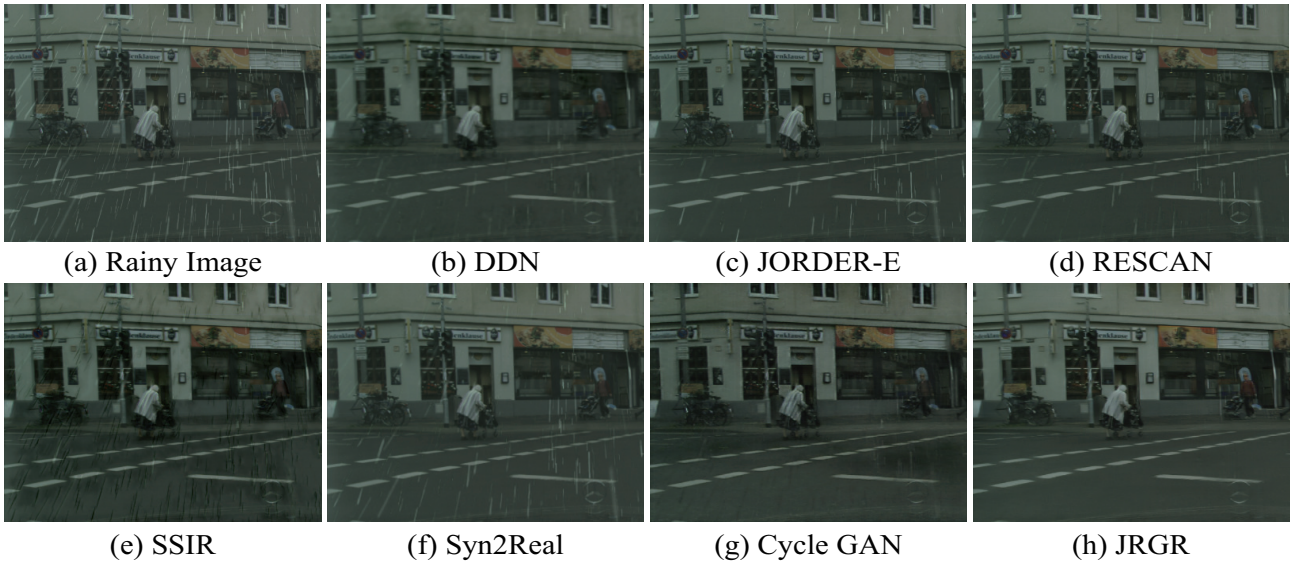


Figure 6. Visualization of deraining results on Rendering dataset.

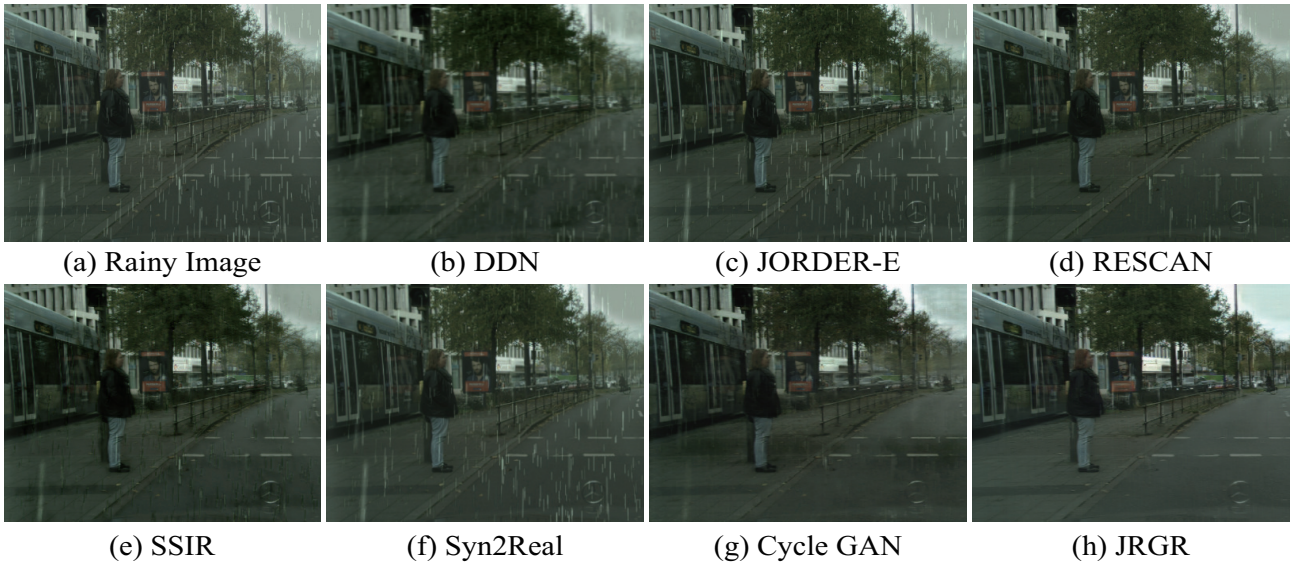


Figure 7. Visualization of deraining results on Rendering dataset.

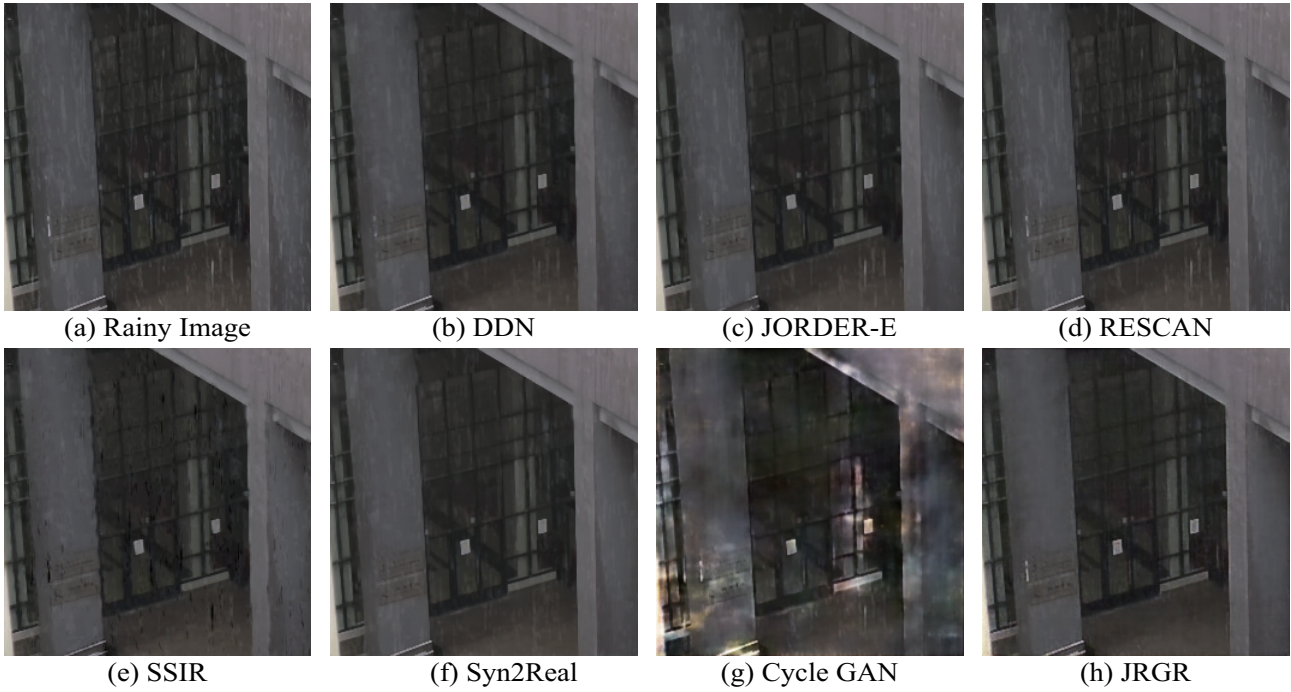


Figure 10. Visualization of deraining results on RainHQ dataset.

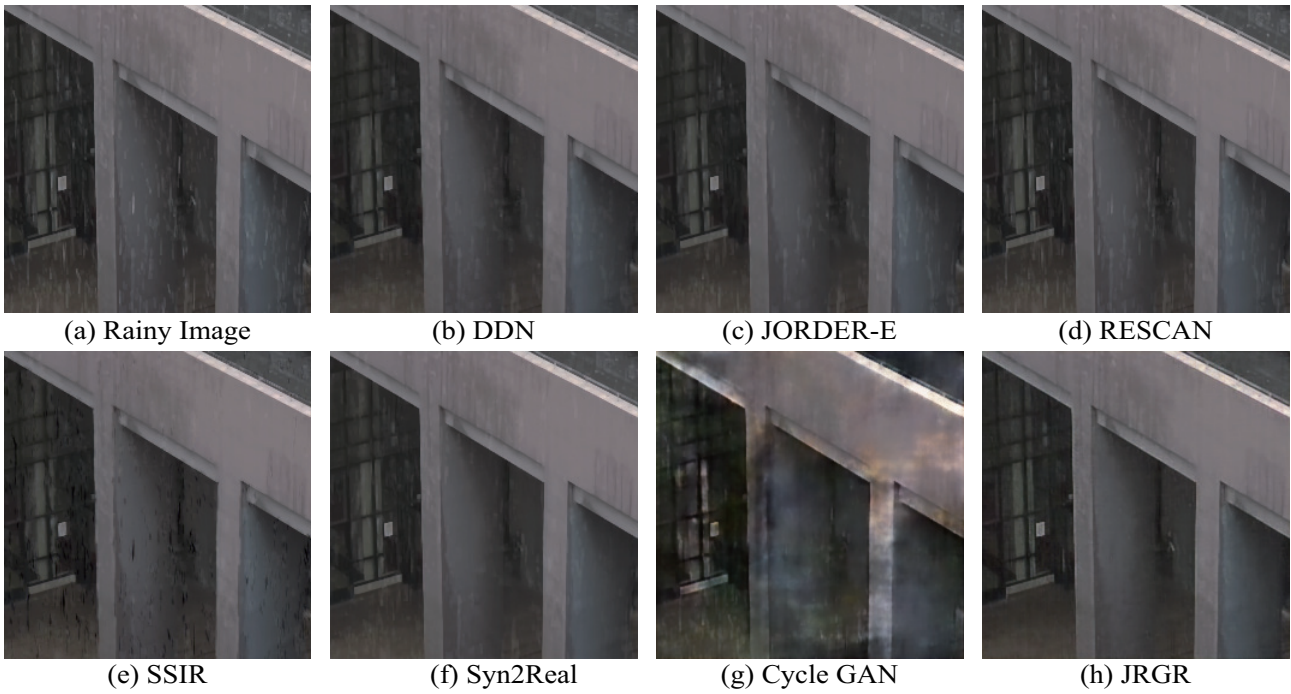


Figure 11. Visualization of deraining results on RainHQ dataset.

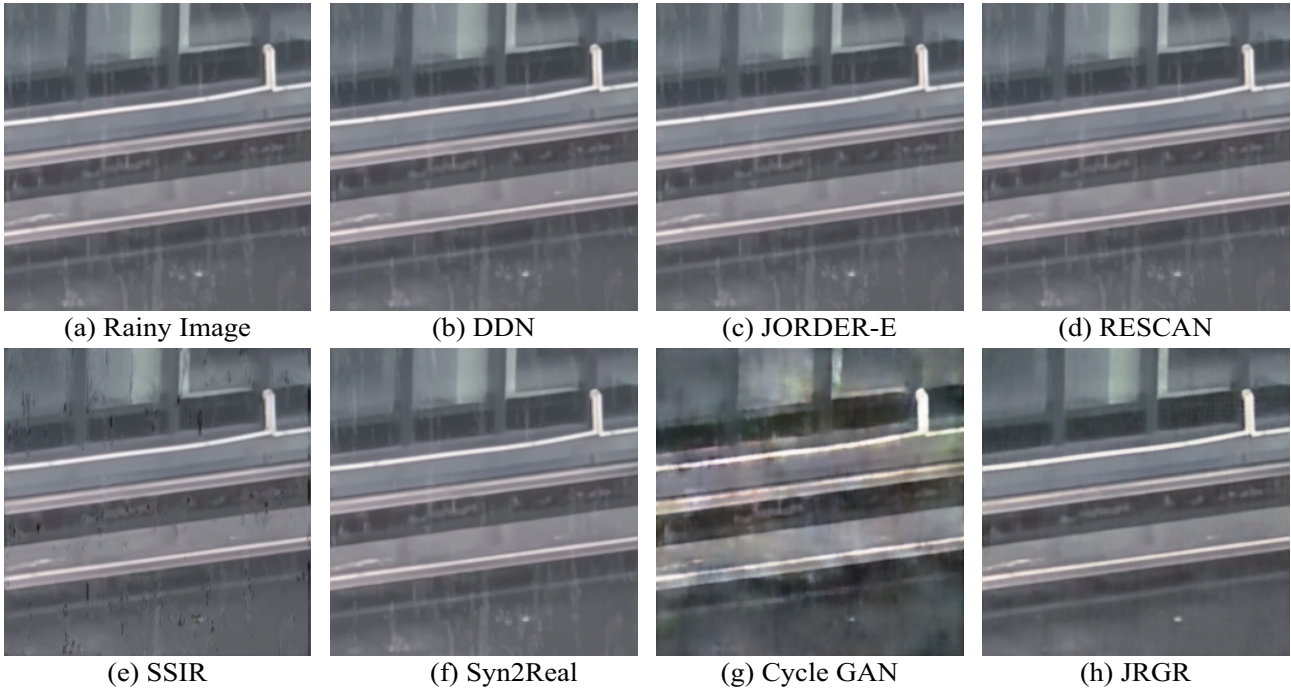


Figure 12. Visualization of deraining results on RainHQ dataset.



Figure 13. Visualization of deraining results on RainHQ dataset.



Figure 14. Illustration of the training data on our collected RealRain. For supervised methods, we utilize (a) paired synthetic data to train the models and test them in (b) unpaired real data. For semi-supervised methods, we train the models with (a) and (b), and test them in (b). For unsupervised methods, we train the models with (b) and the clean images in (a), and test them in (b).

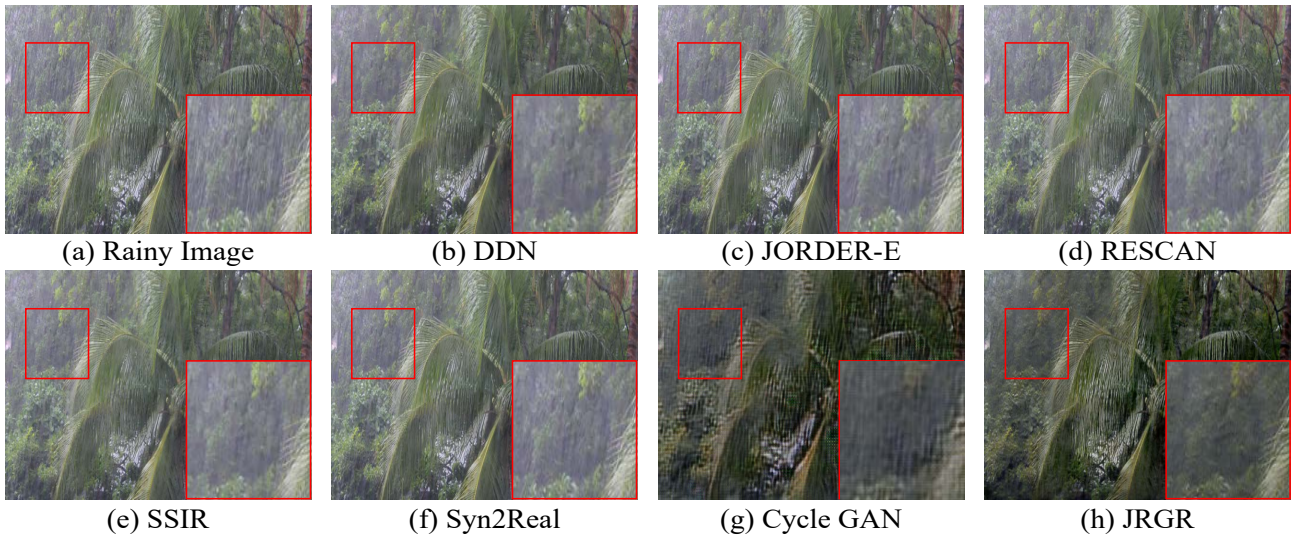


Figure 15. Visualization of deraining results on RainReal dataset.

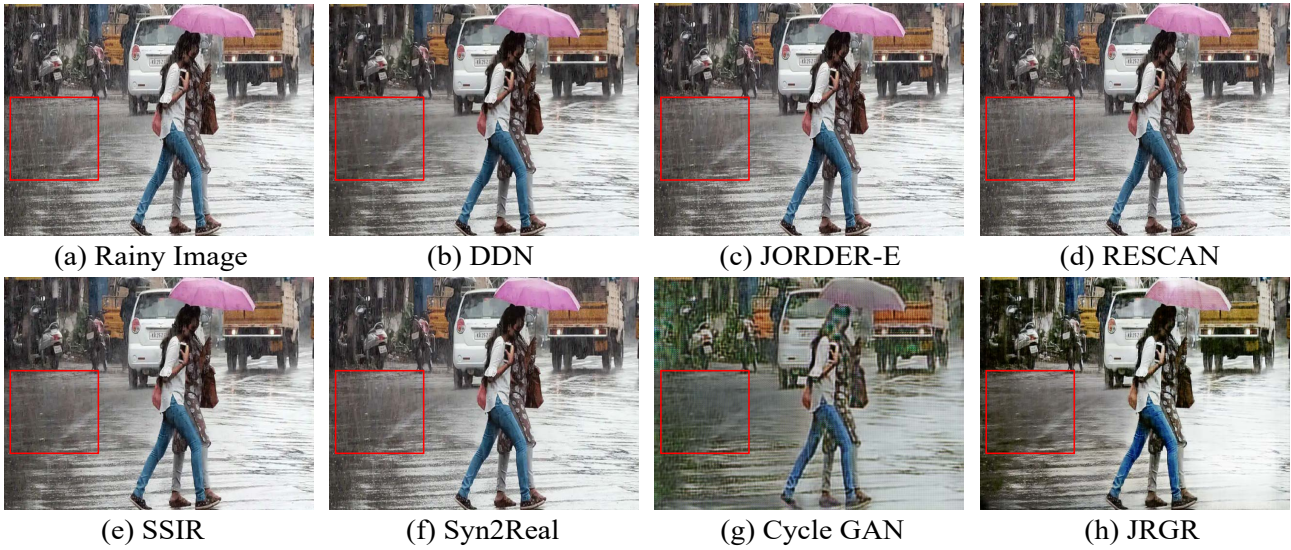


Figure 16. Visualization of deraining results on RainReal dataset.

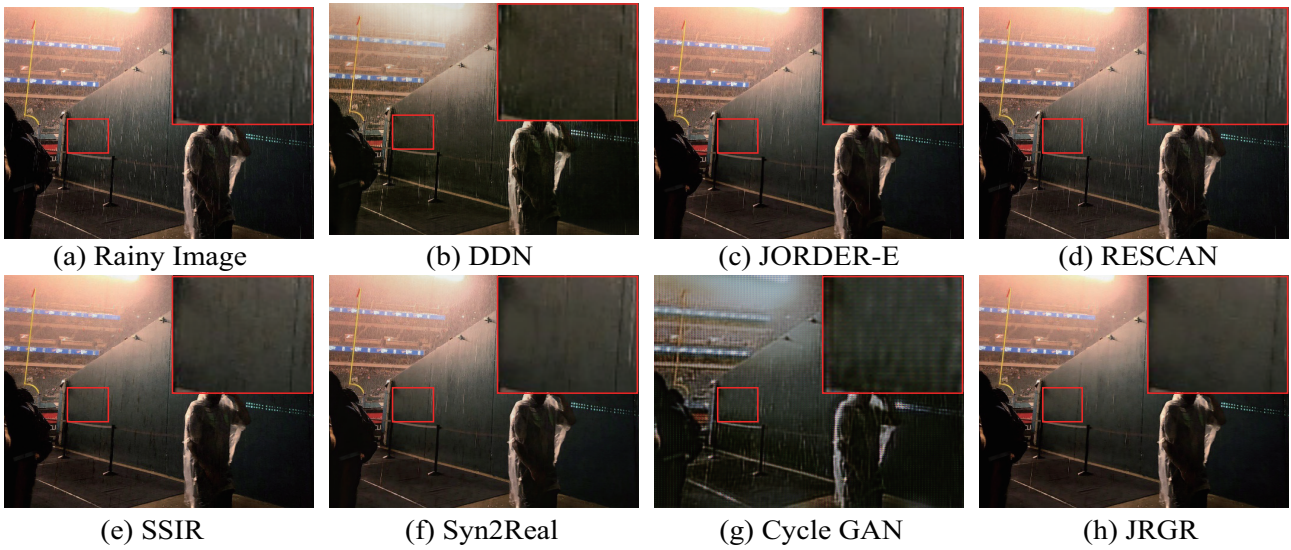


Figure 17. Visualization of deraining results on RainReal dataset.

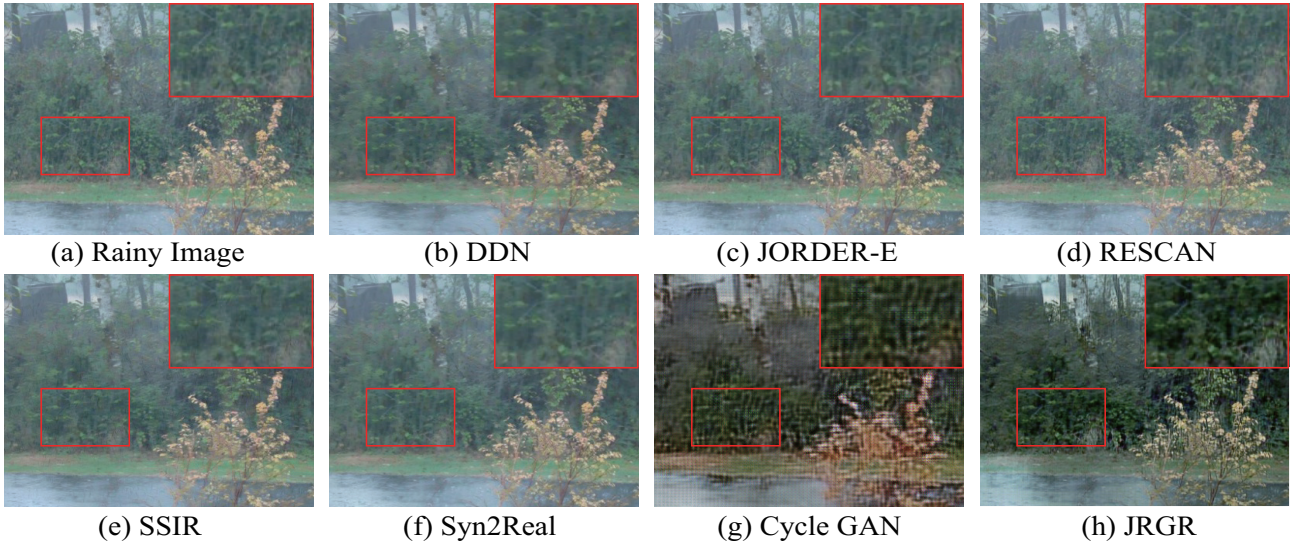


Figure 18. Visualization of deraining results on RainReal dataset.



Figure 19. Visualization of deraining results on RainReal dataset.



(a) Rainy Image

(b) w/o L_{adv}

(c) w/o L_{eye}



(d) w/o L_{MSE}



(d) JRGR

Figure 20. Ablation Study on the effectiveness of different loss functions.



Figure 21. Ablation Study on the effectiveness of different loss functions.



(a) Rainy Image

(b) w/o L_{adv}

(c) w/o L_{cyc}



(d) w/o L_{MSE}



(d) JRGR

Figure 22. Ablation Study on the effectiveness of different loss functions.